PHYSICS

Room-temperature single-photon emitters in silicon nitride

Alexander Senichev[1,2]*†, Zachariah O. Martin[1,2]†, Samuel Peana[1]†, Demid Sychev[1,2], Xiaohui Xu[1,2,3], Alexei S. Lagutchev[1,2], Alexandra Boltasseva[1,2], Vladimir M. Shalaev[1,2]*

Single-photon emitters are essential in enabling several emerging applications in quantum information technology, quantum sensing, and quantum communication. Scalable photonic platforms capable of hosting intrinsic or embedded sources of single-photon emission are of particular interest for the realization of integrated quantum photonic circuits. Here, we report on the observation of room-temperature single-photon emitters in silicon nitride (SiN) films grown on silicon dioxide substrates. Photophysical analysis reveals bright (>10^5 counts/s), stable, linearly polarized, and pure quantum emitters in SiN films with a second-order autocorrelation function value at zero time delay $g^{(2)}(0)$ below 0.2 at room temperature. We suggest that the emission originates from a specific defect center in SiN because of the narrow wavelength distribution of the observed luminescence peak. Single-photon emitters in SiN have the potential to enable direct, scalable, and low-loss integration of quantum light sources with a well-established photonic on-chip platform.

INTRODUCTION

On-chip integrated single-photon sources are key elements in various quantum information systems including emerging protocols in quantum communication, sensing, and computing (*1*–*3*). Room-temperature single-photon emitters (SPEs) that are promising for practical applications have been observed in diamond (*4*, *5*), two-dimensional (2D) hexagonal boron nitride (hBN) (*6*, *7*), and semiconducting carbon nanotubes (*8*), to name a few. Current approaches to realize on-chip quantum emitters rely on hybrid and heterogeneous integration. This integration requires complex geometries and fabrication to combine materials that host SPEs with photonic circuitry (waveguides, couplers, photonic crystal cavities, etc.) (*9*, *10*). Hybrid photonic integration typically faces challenges related to scalability, optical losses, and efficient coupling between different photonic elements on one chip. Although several demonstrations of hybrid integration have been successfully demonstrated, including the large-scale integration of diamond-based quantum emitters with an aluminum nitride photonic platform (*11*), there is still a great need to develop architectures and approaches that use well-established scalable optical circuitry platforms with intrinsic or controllably embedded SPEs (*12*, *13*). So far, intrinsic sources of single-photon emission have been found in wide-bandgap semiconductor materials such as silicon carbide (*14*, *15*), gallium nitride (GaN) (*16*, *17*), and aluminum nitride (AlN) (*18*, *19*), which are promising for the realization of quantum photonic circuitry elements (*20*–*24*).

Among several state-of-the-art quantum photonic platforms, silicon nitride (SiN) has emerged as an attractive material to construct integrated photonic components compatible with the metal-oxide semiconductor process (*25*–*27*). SiN offers a relatively high refractive index ($n \sim 2.0$) and provides the required index contrast with silicon dioxide (SiO_2; $n = 1.5$) for efficient photonic waveguides and other on-chip components. For example, on-chip frequency converters and optical parametric oscillators were realized with SiN-based microring resonators (*28*, *29*). SiN also offers a large transparency window spanning from near-infrared wavelengths down to at least 500 nm. Low-loss SiN waveguides with operation wavelengths in the range of 532 to 1580 nm were demonstrated (*30*, *31*). The transparency window of SiN enables integration with light sources with emission in the visible wavelength range such as colloidal quantum dots (QDs) (*32*), nitrogen vacancies in diamond (*33*), and 2D transition metal dichalcogenides (*34*). However, commonly used stoichiometric Si_3N_4 has relatively strong background emission in the visible range that hinders quantum measurements, particularly regarding SPEs operating in this spectral region (*33*). To make SiN practical for quantum photonic applications in the visible range, nonstoichiometric nitrogen-rich SiN films with low background emission were explored (*35*, *36*). It was shown that nitrogen-rich SiN films grown by plasma-enhanced chemical vapor deposition (PECVD) have substantially lower autofluorescence compared to stoichiometric Si_3N_4 while maintaining a moderate refractive index of ~1.9, suitable for quantum photonic measurements of encapsulated nitrogen vacancy centers (*36*).

In this work, we report on high-purity, room-temperature SPEs observed in SiN grown on SiO_2. This platform is a suitable material combination for enabling integrated photonics that is mature in terms of fabrication, quality control, and integration. The utilization of quantum emitters directly embedded in SiN has the potential to mitigate losses resulting from the low coupling efficiency of emission into cavities and photonic waveguides common in hybrid systems. The reported SPEs were obtained by careful selection of the growth conditions for low autofluorescing SiN that allowed us to observe SPEs. Here, we present the detailed analysis of the photophysical properties of the observed SiN-based SPEs and discuss their possible origin.

[1]School of Electrical and Computer Engineering, Birck Nanotechnology Center and Purdue Quantum Science and Engineering Institute, Purdue University, West Lafayette, IN 47906, USA. [2]The Quantum Science Center (QSC), a National Quantum Information Science Research Center of the U.S. Department of Energy (DOE), Oak Ridge, TN 37931, USA. [3]School of Materials Engineering, Purdue University, West Lafayette, IN 47906, USA.
*Corresponding author. Email: senichev@purdue.edu (A.S.); shalaev@purdue.edu (V.M.S.)
†These authors contributed equally to this work.

RESULTS

Sample preparation

For this study, the SiN films were grown by a special type of PECVD called high-density plasma chemical vapor deposition (HDPCVD). It uses an inductively coupled plasma source to generate a higher plasma density compared to PECVD, which enables deposition at lower temperatures (80° to 150°C), improved quality of low-temperature films, and improved trench fill capability (*37*). To find an acceptable background emission of the SiN in the visible spectral range, a variety of nonstoichiometric SiN films were grown with increasing ratio of N_2-to-SiH_4 fluxes. The dependence of the SiN background fluorescence and refractive index on the growth conditions is provided in the Supplementary Materials (see fig. S1). The SiN films studied in this work were grown on commercially available silicon (Si) substrates topped with a 3-μm-thick SiO_2 layer. The growth on such SiO_2-topped substrates was motivated by their suitability for fabrication of SiN waveguide structures. We have also performed the growth of SiN films on Si substrates coated with a 285-nm-thick SiO_2 film and on bare Si substrates with a native oxide layer for comparison. The results of SPEs' characterization in SiN grown on these substrates may be found in the Supplementary Materials. We performed optical characterization of the bare 3-μm-thick SiO_2 substrates before SiN deposition to evaluate the background fluorescence. The background signal has negligibly low counts with no localized emission centers. The target thickness of SiN films was selected to be about 200 nm. For activation of quantum emitters, thermal annealing is commonly applied for materials such as hBN (*38*). Here, we used rapid thermal annealing (RTA) of the samples after deposition. For this purpose, the samples were heated to 1100°C for 120 s in nitrogen atmosphere using a Jipelec Jetfirst RTA system. We additionally applied thermal annealing at 850°C for 60 min under argon atmosphere in a conventional furnace (Blue M). The alignment markers were fabricated by focused ion beam (FIB) milling to identify emitter positions in consecutive measurements.

Photoluminescence map and surface morphology

Figure 1A shows a typical confocal scanning photoluminescence (PL) intensity map of the SiN layer grown on 3-μm-thick SiO_2, revealing point-like emitters randomly distributed across the sample. The bright cross-like features are alignment markers. The fluorescence from these alignment markers is attributed to FIB-induced incorporation of gallium ions into the SiN film. The optical image of the sample surface with alignment markers is shown in Fig. 1B. The estimated density of quantum emitters was at least one to two emitters per $10 \times 10\ \mu m^2$ area; this is comparable with previously reported quantum emitters in GaN and AlN (*16*, *18*). Figure 1C shows the surface morphology of the SiN film measured by atomic force microscopy (AFM). The surface of SiN sample has a root mean square (rms) roughness of approximately 1.5 nm with the appearance of a grainy surface structure. The comparison of the PL intensity map and the corresponding AFM micrographs does not suggest a direct correlation between the position and the density of emitters and the surface pattern (see fig. S2 for more AFM results at different scales).

Photophysical properties

Below, we show an example of the photophysical analysis of a representative SPE. The position of the emitter was revealed from the PL intensity map (Fig. 2A). Once located, the nonclassical photon

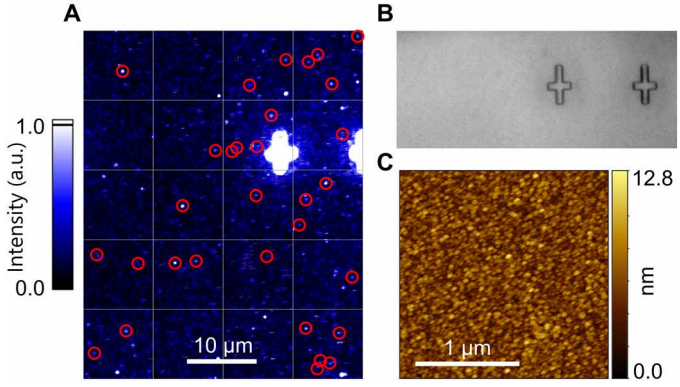

Fig. 1. Room-temperature SPEs in SiN grown on SiO_2-on-Si substrate. (**A**) Confocal PL intensity map of the SiN layer. Confirmed SPEs are indicated with red circles. a.u., arbitrary units. (**B**) Optical image of the sample with markers prepared by the FIB milling to identify the same area in consecutive measurements. (**C**) Representative 2 μm by 2 μm AFM micrograph revealing the surface morphology of the SiN film and yielding the rms roughness of 1.5 nm. Scale bar, 1 μm.

statistics from the selected emitter was confirmed by second-order autocorrelation $g^{(2)}(\tau)$ measurements. Figure 2B shows the $g^{(2)}(\tau)$ histogram recorded under continuous laser excitation. The data were fitted with a three-level model as the $g^{(2)}(\tau)$ histogram exhibits slight bunching at longer time scales with increasing excitation power (see fig. S3 for the excitation power dependence measurements). We obtained the $g^{(2)}(\tau)$ value of 0.12 at zero delay time, indicating a high-purity single-photon source. To assess the average photon purity across many SPEs in SiN, we collected the $g^{(2)}(\tau)$ data from the total of 130 emitters. The results are presented in Fig. 2C. Most of the emitters show $g^{(2)}(0)$ well below the threshold value of 0.5, confirming that the emission is nonclassical and the sources are SPEs. Moreover, the studied SPEs show, on average, high quantum emission purity with a $g^{(2)}(0)$ value of about 0.2. The $g^{(2)}(0)$ values shown in Fig. 2 (B and C) were obtained without any background correction or spectral filtering. This suggests that the real quantum emission purity could be higher than the measurement would indicate. We also measured the fluorescence lifetime for 44 different emitters with pulsed laser excitation. The emission lifetime was found to range from 1.4 to 3.9 ns, with the average value across measured emitters of 2.4 ns. The full results of the emission lifetime measurements are given in the Supplementary Materials (fig. S4).

Next, we address the spectral characteristics of the selected SPE. The corresponding PL spectrum is shown in Fig. 3A. The PL data were background-corrected and normalized to the maximum intensity. The PL spectrum consists of several peaks that can be well fitted with four Gaussian line shapes. The most intense PL peak is accompanied with satellite peaks of lower intensity on both sides. The presented PL spectrum of the SPE in SiN appears to be different from typical PL spectra of SPEs in crystalline hBN (*6*), GaN (*16*, *39*), and AlN (*18*, *19*) that exhibit a prominent zero-phonon line and lower-intensity red-shifted phonon sidebands. This indicates the different possible origins of the emitters and/or effects of the amorphous SiN matrix. To gain a better understanding of the structure of the PL spectra and PL peak distribution, we analyzed the PL data from several SPEs as discussed below.

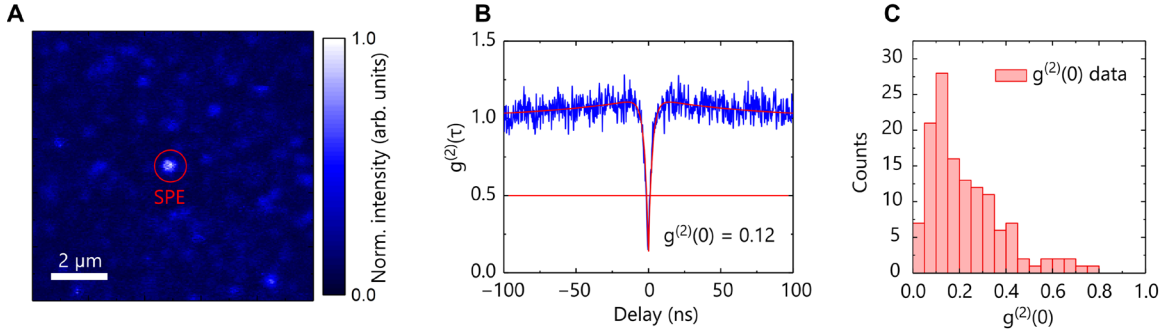

Fig. 2. Purity of single-photon emission in SiN. (**A**) Confocal PL map of the SPE. (**B**) Second-order autocorrelation measurement $g^{(2)}(\tau)$ of the emission, yielding $g^{(2)}(0)$ of 0.12. (**C**) Histogram of $g^{(2)}(0)$ distribution from 130 emitters with a bin size of 0.05.

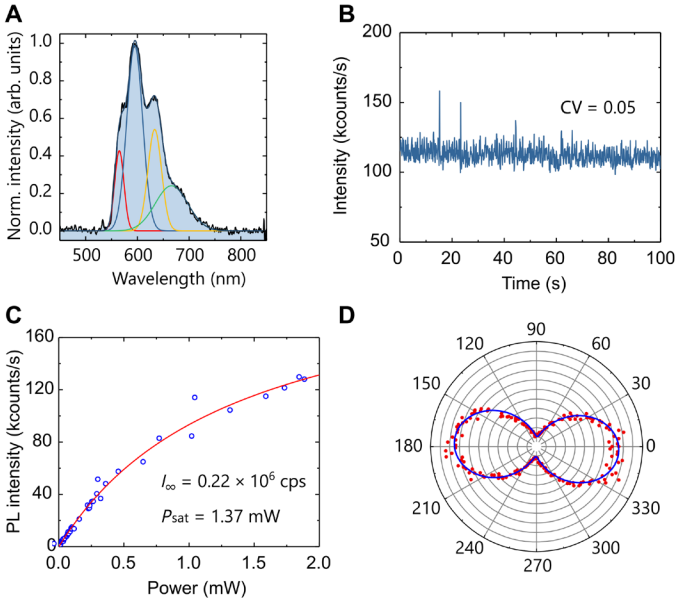

Fig. 3. Photophysical characteristics of SPEs in SiN measured at room temperature. (**A**) PL spectrum with four Gaussian-fitted line shapes. (**B**) PL stability measurement showing no obvious blinking or bleaching and a low coefficient of variation CV = 0.05. (**C**) Saturation curve yielding a saturation power of P_{sat} = 1.37 mW and intensity $I_\infty = 0.22 \times 10^6$ counts/s (cps). (**D**) Polarization diagram of the PL emission $I(\theta)$ (measured from another emitter). The data are fitted with $a\cos^2(\theta)$-form fit function, yielding the polarization visibility $(I_{max} - I_{min})/(I_{max} + I_{min})$ of 78%.

For the SPE shown in Fig. 2A, we assessed such essential metrics of quantum emitters as stability, brightness, and emission rate. The selected emitter exhibits stable emission without obvious blinking or bleaching over a measurement period of 100 s under near-saturation excitation power (1.4 mW) as demonstrated in Fig. 3B. The PL stability is quantified with a coefficient of variation CV = σ/μ, where σ is the SD and μ is the mean value of the PL intensity during measurements. For this particular emitter, we obtained a variation of PL intensity of 0.05. Such behavior is observed for most of the emitters. However, some SPEs showed blinking and switching between "on" and "off" states (see fig. S5 for details). The saturation behavior of the emission as a function of excitation power $I(P)$ is shown in Fig. 3C. The data were fitted with the equation $I(P) = I_\infty \times P/(P + P_{sat})$, where I_∞ and P_{sat} are fitting parameters corresponding to the maximum count and saturation power, respectively. We obtained an emitter brightness of $I_\infty = 0.22 \times 10^6$ counts/s at a saturation power of P_{sat} = 1.37 mW (measured before the objective). The background fluorescence intensity at the same excitation power was on the order of 0.2×10^5 counts/s. The observed emitter brightness was comparable to the room-temperature emission from SPEs in III-nitride semiconductors (*16*, *18*, *19*).

In addition, we measured the polarization dependence of emission from SPEs in SiN. The polarization diagram of the PL emission $I(\theta)$ of an emitter is shown in Fig. 3D as an example. The polarization diagrams of additional emitters are given in the Supplementary Materials (fig. S6). The results indicate that the emission originates from linearly polarized dipole transitions. The Supplementary Materials (fig. S7) also contain a comprehensive photophysical analysis of an additional SPE in SiN.

Spectral characteristics

We further analyzed the SPEs PL spectra. In Fig. 4A, the emission spectrum for another SPE exhibits slightly different spectral characteristics, having only three PL peaks compared to the one in Fig. 3. In total, we analyzed the emission spectra of 133 individual SPEs with the best signal-to-noise ratio recorded from different scans and three independently fabricated samples. The data were fitted with the Gaussian line shapes to assess the spectral characteristics of the PL peaks. We found that most of the emitters exhibit emission spectra composed of PL peaks of nearly the same wavelength. Figure 4B shows a histogram of the wavelength distribution for these emitters. The PL peaks are clustered around E_1 = 567 nm, E_2 = 596 nm, E_3 = 632 nm, and E_4 = 670 nm with SD values of 6, 7, 9, and 10 nm, respectively. The most intense PL peak in these spectra is typically at one of the two central wavelengths. The observed fluctuation of the PL peak wavelength could be attributed to variations in the surrounding SiN matrix. A detailed analysis of some representative PL spectra of these SPEs can be found in the Supplementary Materials (figs. S8 and S9). We found that there are also emitters showing long-wavelength PL peaks above 700 nm (for details, see figs. S11 and S12). These emitters are much less frequent than those showing PL peaks around the wavelength indicated in Fig. 4B.

As was mentioned above, SiN films were also grown on Si substrates topped by a 285-nm-thick SiO_2 and on bare Si substrates with a native oxide layer. The SPEs on bare Si substrates are rare, which precludes statistical analysis of their photophysical properties (for

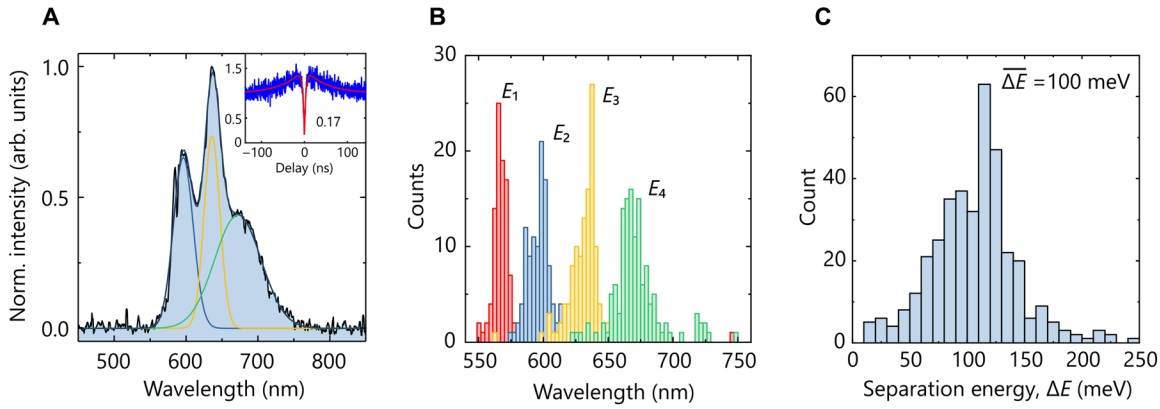

Fig. 4. Spectral analysis of SPEs in SiN. (**A**) Representative PL spectrum of an SPE. PL spectra can be well fitted with Gaussian line shapes. Inset: Second-order autocorrelation measurements of the emission from the corresponding emitter. (**B**) Histogram of the wavelength distribution of 133 emitters with a bin width of 3 nm. (**C**) Histogram of the distribution of the separation energy ΔE obtained for all peaks resolved in PL spectra. The average separation energy is 100 meV. The bin width is 10 meV.

details, see fig. S14). The density of SPEs in SiN grown on 285-nm-thick SiO_2 is comparable to that of SPEs on 3-μm-thick SiO_2. Their PL spectra also exhibit a multipeak nature that can be fitted with four Gaussian line shapes clustering at specific wavelengths (fig. S15). The direct comparison of the selected PL spectra from SPEs in SiN grown on 3-μm-thick and 285-nm-thick SiO_2, respectively, as well as histograms of the wavelength distribution demonstrate the similar nature of their spectral properties in terms of the occurrence of multiple peaks. Because SPEs in SiN grown on 3-μm-thick and 285-nm-thick SiO_2 substrates both exhibit multiline PL spectra, the oscillations in the SPE emission spectrum are likely the intrinsic property of these quantum emitters rather than the interference effect of Fabry-Perot resonances. The difference in the SiO_2 thickness between these two substrates is one order of magnitude. Such difference would markedly change the spectral separation of Fabry-Perot interference fringes, while the PL peak separations for SPEs on both substrates are comparable. It can be noted that PL spectra of SPEs in SiN on 285-nm-thick SiO_2 are overall blue-shifted compared to those on 3-μm-thick SiO_2. The origin of this spectral shift might be related to slightly different properties of the SPEs created on these two substrates because the properties of SiO_2 might vary.

In addition, we also addressed the multiline nature of the PL spectra by performing wavelength-resolved detection of single photons. For these experiments, we selected an SPE with a characteristic PL spectrum as shown in Fig. 5B. The second-order autocorrelation function $g^{(2)}$ was measured for the full spectrum and the selected wavelength ranges. The $g^{(2)}$ values at zero delay time are presented in Fig. 5C. It appears that single-photon emission persists within each selected spectral band. Furthermore, the value of the $g^{(2)}$ second-order autocorrelation function dip at zero delay time for different spectral lines remains essentially the same within experimental uncertainty.

Nature of quantum emitters in SiN

Here, we discuss the possible origin of the observed quantum emitters. We studied the formation of SPEs in SiN grown on different substrates. The obtained results indicate that the growth on Si substrates with grown SiO_2 layers promotes the formation of SPEs in SiN after RTA treatment. These findings suggest the possible formation of optically active defects at the interface between SiN and SiO_2 layers; however, further studies are required to firmly establish such dependence. Because the position of the emission lines in PL spectra are at virtually identical wavelengths for multiple SPEs (Fig. 4B), the observed single-photon emission from the SiN can be associated with the same source. The origin of luminescence in SiN systems has been extensively studied in the past for their applications in Si-based optoelectronic devices. PL emission from SiN films in the visible range has been previously attributed to both the quantum confinement effect of carriers inside Si QDs embedded in the SiN and radiative defect–related states in SiN or at Si-QD/SiN interface structures (*40*, *41*). PL peaks exhibiting spectral shifts with annealing temperature and SiN composition were typically associated with the Si QDs. In QDs, the energy levels are defined by the quantum confinement effect and, hence, sensitive to the changes in the nanoparticles' size and morphology due to thermal annealing and composition variations (*40*, *41*). However, the QD-related PL spectra were typically reported for SiN films with the high Si composition, possibly resulting in the Si nanoparticle formation (*41*). In contrast, the SiN samples studied in this work were grown in the nitrogen-rich regime. Moreover, the emission lifetime for Si QDs in SiN was found to be on the order of microseconds (*41*), which is substantially longer than that observed for the SPEs in this work. Therefore, we suggest that the origin of studied SPEs in SiN is unlikely to be related to the quantum confinement effect of the carriers in Si nanoparticles formed within the SiN matrix.

The PL peaks that show no changes with the composition of SiN films or annealing temperatures were previously attributed to radiative defect states (*41*). In this case, the PL emission depends only on the energy level of a particular defect. The PL spectra of defect-related emissions reported in the literature for SiN films also show a multipeak nature similar to our work (*40*–*42*). One notable similarity is the appearance of a strong central PL peak with satellites on both sides. The PL peaks are less pronounced compared to our work because the emission was measured from an ensemble of emitters, while we addressed SPEs individually using confocal microscopy. The emission lifetime for SiN SPEs and defect-related emission from SiN reported in the literature are both on the scale of a few nanoseconds. The defect-related emission was attributed to defects existing within Si—Si and N—N bonds and formed by Si and N dangling bonds (*43*). However, the exact nature of defects responsible for the single-photon emission observed in our work requires further study.

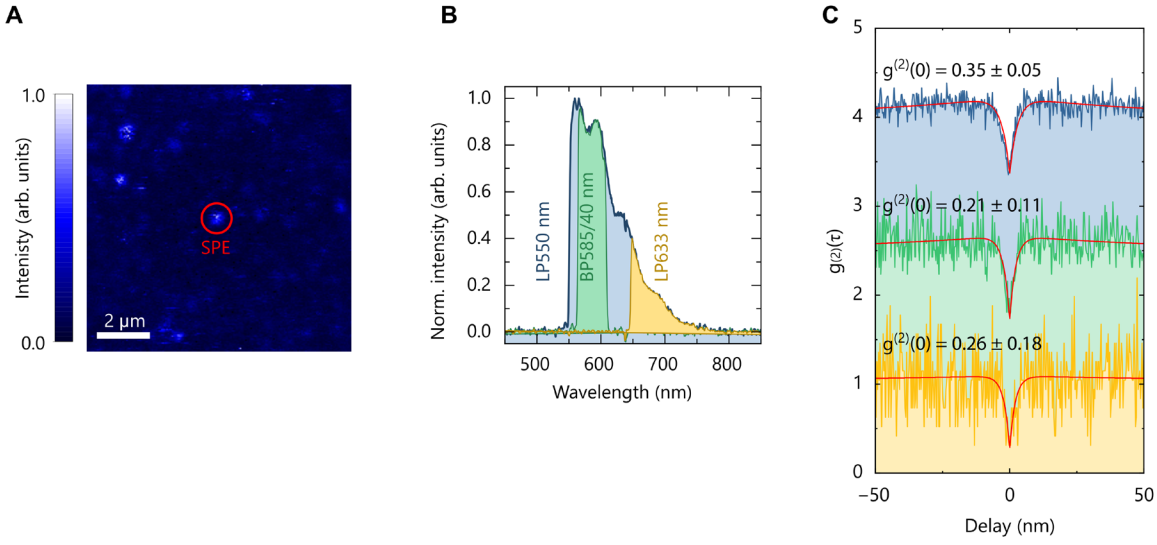

Fig. 5. Wavelength-resolved detection of single photons. (**A**) Confocal PL map of the SPE. (**B**) PL spectrum of the selected SPE. The PL spectra measured using different spectral filters (Band Pass BP585/40nm and Long Pass LP633 nm) are normalized and superimposed with the full spectrum (LP550 nm). (**C**) Second-order autocorrelation measurements $g^{(2)}(\tau)$ of the emission taken using different spectral filters, yielding $g^{(2)}(0)$ of 0.35 ± 0.05 (top), 0.21 ± 0.11 (middle), and 0.26 ± 0.18 (bottom).

Note that, in previous works, the defect-related emission was measured from ensembles. Properties of individual defects acting as SPE were not reported, while, in our work, we demonstrated SPEs in SiN samples.

Multipeak spectra and the short PL lifetimes were also previously observed for individual Si nanocrystals (*44*, *45*) and SiO_2 nanoparticles (*46*) embedded in a polymer matrix. The emission lifetime was found to be between 1 and 13 ns (*45*). In both cases, the emission in these materials was associated with the defect centers in SiO_2. For Si nanocrystals, an SiO_2 shell is typically formed around the Si core because of natural oxidation. In this case, the defect-related emitters exist either at the SiO_2/Si interface or in the SiO_2 shell of small Si nanocrystals. The PL lines were attributed to a zero-phonon band and two low-energy phonon sidebands, which are different from the PL spectra of SiN SPEs in our work. The characteristic PL spectra of SiN SPEs exhibit the most intense PL peak accompanied with satellite peaks of lower intensity on both sides. The single-photon emission characteristics were not studied for these polymer-embedded emitters. Lately, emission spectra with multiple peaks and lifetimes on the order of a few nanoseconds were also reported for bare silica microscope coverslips made of borosilicate glass or fused quartz (*47*). The emission from defects in silica was found to exhibit antibunching, indicating that it originated from the SPE centers. However, the emission of SPEs in silica and those found in SiN samples also exhibits substantial spectral differences. First, the defect-related PL spectra in silica exhibit an intense first peak, which is attributed to the zero-phonon line accompanied by a couple of longer-wavelength phonon sidebands (*47*). The PL spectra of the SPEs in SiN have the satellite PL peaks on both sides of the main peak. Second, the splitting between the zero-phonon band and phonon sidebands in silica samples was found to be between 140 and 180 meV, which can be attributed to the energy of longitudinal optical phonons in SiO_2 at 156 meV (*45*, *47*). The emitters found in SiN samples show, on average, the splitting energy between PL peaks of about 100 meV as shown in Fig. 4C. This value is clearly lower than the separation of the emission lines of SPEs in silica. Besides the spectral differences compared with our SiN SPEs, these three-peak spectra with a zero-phonon line and phonon sidebands are similar to those recently attributed to accidental contamination of dielectric substrates or polymer matrices with organic molecules (*48*). Note that we measured the optical properties of bare SiO_2 (3 μm)–on–Si wafers used for SiN deposition. We characterized these wafers before and after thermal annealing, and no SPEs were observed.

DISCUSSION

Considering SiN SPEs in the broader context of other room-temperature SPEs, the photophysical characteristics of SiN-based quantum emitters are on par with those found in GaN (*16*), AlN (*18*, *19*), and silica (*47*). Their room-temperature operation makes them promising candidates for rapid characterization and practical applications. SiN SPEs exhibit high single-photon purity observed without spectral filtering or background correction. The average $g^{(2)}(0)$ value from 130 SiN SPEs is about 0.2, and the lowest observed value was 0.03. An emission rate exceeding 10^5 counts/s observed from SiN quantum emitters is also typical for SPEs in materials with a high refractive index, such as III-nitrides. The high refractive index of bulk materials typically means poor collection efficiencies. However, the light extraction efficiency from such SPEs can be improved by using patterned substrates that provide the increased reflection area (*17*). Diverse quantum information technology (QIT) applications that could use SPEs impose different requirements on SPE properties and characteristics that may include photon purity $g^{(2)}(0)$, indistinguishability, and efficiency (*1*). For example, high efficiency and small $g^{(2)}(0) < 0.1$ are required for the realization quantum key distribution (QKD), while indistinguishability is not considered to be a critical parameter for some of the suggested QKD schemes (*49*). Because SiN SPEs show excellent $g^{(2)}(0)$ values at room

temperature and without spectral filtering or background correction, they could be excellent sources of single photons for applications, which do not require indistinguishability (*50*). SiN SPEs offer a possibility of monolithic integration with photonic circuitry where high extraction efficiency from an SPE to an optical fiber can be achieved. In addition, on-chip SiN microring resonators were shown to exhibit efficient single-photon-level frequency conversion to telecom range (*28*). Last, embedding SiN SPEs into photonic cavities may provide both emission rate enhancement and spectral filtering of the SPE-generated stream of photons to partially alleviate the multipeak nature of PL emission, thus making SiN SPEs suitable candidates for other QIT applications.

Future research directions include emission enhancement through coupling SiN SPEs to on-chip plasmonic nanostructures previously demonstrated for quantum emitters in nanodiamonds (*51*). However, the quantum emitters found in SiN are excellent candidates for monolithic integration with SiN/SiO_2-based photonic integrated circuits. Last, addressing spin properties of SiN emitters is of particular interest for future research, as optically addressable spins have great potential to enable a variety of applications in quantum information processing and quantum sensing (*52*).

In conclusion, we report on the observed bright, stable, linearly polarized, and high-purity sources of single-photon emission at room temperature in SiN thin films. These SPEs are produced by HDPCVD growth of SiN on SiO_2-coated Si substrates and subsequent RTA. We found that most studied emitters exhibit PL peaks at virtually the same wavelengths, suggesting that the emission likely comes from one particular type of defect center. We hypothesize that these defect centers can be intrinsic to SiN or exist at the SiN/SiO_2 interface. Our findings will spark further studies toward deeper understanding of the origin of SiN-based SPEs. The proposed material platform would allow for scalable integration of SPEs with on-chip quantum photonic circuitry.

MATERIALS AND METHODS

Optical characterization

The optical characterization of SPEs in SiN was performed at room temperature. We used a custom-made scanning confocal microscope based on a commercial inverted microscope body (Ti-U, Nikon). The microscope was equipped with a 100-μm pinhole and an air objective having a numerical aperture of 0.90. We used a continuous-wave 532-nm diode-pumped solid-state laser [lambda beam PB 532-200 diode-pumped solid-state laser (DPSS), RGB Photonics] for optical excitation of emitters. The excitation light and PL signal were separated by a 550-nm long-pass dichroic mirror (DMLP550L, Thorlabs). The remaining pump power was filtered out by a 550-nm long-pass filter (FEL0550, Thorlabs) installed in front of detectors. For the wavelength-resolved detection of single photons, we also used a band-pass filter with a passband from 565 to 605 nm and a long-pass filter with a cut-on wavelength at 633 nm. For lifetime measurements, we used a dispersion-compensated Ti:Sapphire mode-locked laser oscillator with a nominal 80-MHz repetition rate and a pulse duration of about 200 fs at the microscope objective sample plane (Mai Tai DeepSee, Spectra-Physics). The laser output was frequency-doubled to generate excitation wavelength at 520 nm. To reveal the quantum nature of emitters, second-order autocorrelation function [$g^{(2)}$] measurements were performed using the Hanbury-Brown and Twiss setup. The optical setup was described in detail elsewhere (*53*, *54*).

SUPPLEMENTARY MATERIALS

Supplementary material for this article is available at https://science.org/doi/10.1126/sciadv.abj0627

REFERENCES AND NOTES

1. I. Aharonovich, D. Englund, M. Toth, Solid-state single-photon emitters. *Nat. Photonics* **10**, 631–641 (2016).
2. R. Uppu, F. T. Pedersen, Y. Wang, C. T. Olesen, C. Papon, X. Zhou, L. Midolo, S. Scholz, A. D. Wieck, A. Ludwig, P. Lodahl, Scalable integrated single-photon source. *Sci. Adv.* **6**, eabc8268 (2020).
3. M. Davanco, J. Liu, L. Sapienza, C. Z. Zhang, J. V. De Miranda Cardoso, V. Verma, R. Mirin, S. W. Nam, L. Liu, K. Srinivasan, Heterogeneous integration for on-chip quantum photonic circuits with single quantum dot devices. *Nat. Commun.* **8**, 889 (2017).
4. I. Aharonovich, S. Castelletto, D. A. Simpson, C.-H. Su, A. D. Greentree, S. Prawer, Diamond-based single-photon emitters. *Rep. Prog. Phys.* **74**, 076501 (2011).
5. T. Iwasaki, Y. Miyamoto, T. Taniguchi, P. Siyushev, M. H. Metsch, F. Jelezko, M. Hatano, Tin-vacancy quantum emitters in diamond. *Phys. Rev. Lett.* **119**, 253601 (2017).
6. T. T. Tran, K. Bray, M. J. Ford, M. Toth, I. Aharonovich, Quantum emission from hexagonal boron nitride monolayers. *Nat. Nanotechnol.* **11**, 37–41 (2016).
7. A. Gottscholl, M. Kianinia, V. Soltamov, S. Orlinskii, G. Mamin, C. Bradac, C. Kasper, K. Krambrock, A. Sperlich, M. Toth, I. Aharonovich, V. Dyakonov, Initialization and read-out of intrinsic spin defects in a van der Waals crystal at room temperature. *Nat. Mater.* **19**, 540–545 (2020).
8. X. Ma, N. F. Hartmann, J. K. S. Baldwin, S. K. Doorn, H. Htoon, Room-temperature single-photon generation from solitary dopants of carbon nanotubes. *Nat. Nanotechnol.* **10**, 671–675 (2015).
9. A. W. Elshaari, W. Pernice, K. Srinivasan, O. Benson, V. Zwiller, Hybrid integrated quantum photonic circuits. *Nat. Photonics* **14**, 285–298 (2020).
10. J. Wang, F. Sciarrino, A. Laing, M. G. Thompson, Integrated photonic quantum technologies. *Nat. Photonics* **14**, 273–284 (2020).
11. N. H. Wan, T.-J. Lu, K. C. Chen, M. P. Walsh, M. E. Trusheim, L. De Santis, E. A. Bersin, I. B. Harris, S. L. Mouradian, I. R. Christen, E. S. Bielejec, D. Englund, Large-scale integration of artificial atoms in hybrid photonic circuits. *Nature* **583**, 226–231 (2020).
12. B. J. M. Hausmann, B. Shields, Q. Quan, P. Maletinsky, M. McCutcheon, J. T. Choy, T. M. Babinec, A. Kubanek, A. Yacoby, M. D. Lukin, M. Lončar, Integrated diamond networks for quantum nanophotonics. *Nano Lett.* **12**, 1578–1582 (2012).
13. M. Schwartz, E. Schmidt, U. Rengstl, F. Hornung, S. Hepp, S. L. Portalupi, K. Llin, M. Jetter, M. Siegel, P. Michler, Fully on-chip single-photon Hanbury-Brown and twiss experiment on a monolithic semiconductor–superconductor platform. *Nano Lett.* **18**, 6892–6897 (2018).
14. B. Lienhard, T. Schröder, S. Mouradian, F. Dolde, T. T. Tran, I. Aharonovich, D. Englund, Bright and photostable single-photon emitter in silicon carbide. *Optica* **3**, 768 (2016).
15. J. Wang, Y. Zhou, Z. Wang, A. Rasmita, J. Yang, X. Li, H. J. von Bardeleben, W. Gao, Bright room temperature single photon source at telecom range in cubic silicon carbide. *Nat. Commun.* **9**, 4106 (2018).
16. A. M. Berhane, K.-Y. Y. Jeong, Z. Bodrog, S. Fiedler, T. Schröder, N. V. Triviño, T. Palacios, A. Gali, M. Toth, D. Englund, I. Aharonovich, Bright room-temperature single-photon emission from defects in gallium nitride. *Adv. Mater.* **29**, 1605092 (2017).
17. Y. Zhou, Z. Wang, A. Rasmita, S. Kim, A. Berhane, Z. Bodrog, G. Adamo, A. Gali, I. Aharonovich, W.-B. Gao, Room temperature solid-state quantum emitters in the telecom range. *Sci. Adv.* **4**, eaar3580 (2018).
18. S. G. Bishop, J. P. Hadden, F. D. Alzahrani, R. Hekmati, D. L. Huffaker, W. W. Langbein, A. J. Bennett, Room temperature quantum emitter in aluminum nitride. *ACS Photonics* **7**, 1636–1641 (2020).
19. Y. Xue, H. Wang, N. Xie, Q. Yang, F. Xu, B. Shen, J. Shi, D. Jiang, X. Dou, T. Yu, B. Sun, Single-photon emission from point defects in aluminum nitride films. *J. Phys. Chem. Lett.* **11**, 2689–2694 (2020).
20. A. L. Crook, C. P. Anderson, K. C. Miao, A. Bourassa, H. Lee, S. L. Bayliss, D. O. Bracher, X. Zhang, H. Abe, T. Ohshima, E. L. Hu, D. D. Awschalom, Purcell enhancement of a single silicon carbide color center with coherent spin control. *Nano Lett.* **20**, 3427–3434 (2020).
21. D. M. Lukin, M. A. Guidry, J. Vučković, Integrated quantum photonics with silicon carbide: Challenges and prospects. *PRX Quantum* **1**, 020102 (2020).
22. Y. Zhang, L. McKnight, E. Engin, I. M. Watson, M. J. Cryan, E. Gu, M. G. Thompson, S. Calvez, J. L. O'Brien, M. D. Dawson, GaN directional couplers for integrated quantum photonics. *Appl. Phys. Lett.* **99**, 161119 (2011).
23. T.-J. Lu, M. Fanto, H. Choi, P. Thomas, J. Steidle, S. Mouradian, W. Kong, D. Zhu, H. Moon, K. Berggren, J. Kim, M. Soltani, S. Preble, D. Englund, Aluminum nitride integrated photonics platform for the ultraviolet to visible spectrum. *Opt. Express* **26**, 11147–11160 (2018).

24. T.-J. Lu, B. Lienhard, K.-Y. Jeong, H. Moon, A. Iranmanesh, G. Grosso, D. Englund, Bright high-purity quantum emitters in aluminum nitride integrated photonics. *ACS Photonics* **7**, 2650–2657 (2020).
25. X. Lu, Q. Li, D. A. Westly, G. Moille, A. Singh, V. Anant, K. Srinivasan, Chip-integrated visible–telecom entangled photon pair source for quantum communication. *Nat. Phys.* **15**, 373–381 (2019).
26. A. L. Gaeta, M. Lipson, T. J. Kippenberg, Photonic-chip-based frequency combs. *Nat. Photonics* **13**, 158–169 (2019).
27. D. Awschalom, K. K. Berggren, H. Bernien, S. Bhave, L. D. Carr, P. Davids, S. E. Economou, D. Englund, A. Faraon, M. Fejer, S. Guha, M. V. Gustafsson, E. Hu, L. Jiang, J. Kim, B. Korzh, P. Kumar, P. G. Kwiat, M. Lončar, M. D. Lukin, D. A. B. Miller, C. Monroe, S. W. Nam, P. Narang, J. S. Orcutt, M. G. Raymer, A. H. Safavi-Naeini, M. Spiropulu, K. Srinivasan, S. Sun, J. Vučković, E. Waks, R. Walsworth, A. M. Weiner, Z. Zhang, Development of quantum interconnects (QuICs) for next-generation information technologies. *PRX Quantum* **2**, 017002 (2021).
28. Q. Li, M. Davanço, K. Srinivasan, Efficient and low-noise single-photon-level frequency conversion interfaces using silicon nanophotonics. *Nat. Photonics* **10**, 406–414 (2016).
29. Y. Okawachi, M. Yu, J. K. Jang, X. Ji, Y. Zhao, B. Y. Kim, M. Lipson, A. L. Gaeta, Demonstration of chip-based coupled degenerate optical parametric oscillators for realizing a nanophotonic spin-glass. *Nat. Commun.* **11**, 4119 (2020).
30. A. Z. Subramanian, P. Neutens, A. Dhakal, R. Jansen, T. Claes, X. Rottenberg, F. Peyskens, S. Selvaraja, P. Helin, B. DuBois, K. Leyssens, S. Severi, P. Deshpande, R. Baets, P. Van Dorpe, Low-loss singlemode PECVD silicon nitride photonic wire waveguides for 532–900 nm wavelength window fabricated within a CMOS pilot line. *IEEE Photonics J.* **5**, 2202809 (2013).
31. Y. Huang, J. Song, X. Luo, T.-Y. Liow, G.-Q. Lo, CMOS compatible monolithic multi-layer Si_3N_4-on-SOI platform for low-loss high performance silicon photonics dense integration. *Opt. Express* **22**, 21859–21865 (2014).
32. W. Xie, Y. Zhu, T. Aubert, S. Verstuyft, Z. Hens, D. Van Thourhout, Low-loss silicon nitride waveguide hybridly integrated with colloidal quantum dots. *Opt. Express* **23**, 12152–12160 (2015).
33. S. L. Mouradian, T. Schröder, C. B. Poitras, L. Li, J. Goldstein, E. H. Chen, M. Walsh, J. Cardenas, M. L. Markham, D. J. Twitchen, M. Lipson, D. Englund, Scalable integration of long-lived quantum memories into a photonic circuit. *Phys. Rev. X* **5**, 031009 (2015).
34. F. Peyskens, C. Chakraborty, M. Muneeb, D. Van Thourhout, D. Englund, Integration of single photon emitters in 2D layered materials with a silicon nitride photonic chip. *Nat. Commun.* **10**, 4435 (2019).
35. A. Gorin, A. Jaouad, E. Grondin, V. Aimez, P. Charette, Fabrication of silicon nitride waveguides for visible-light using PECVD: A study of the effect of plasma frequency on optical properties. *Opt. Express* **16**, 13509–13516 (2008).
36. J. Smith, J. Monroy-Ruz, J. G. Rarity, K. C. Balram, Single photon emission and single spin coherence of a nitrogen vacancy center encapsulated in silicon nitride. *Appl. Phys. Lett.* **116**, 134001 (2020).
37. J. W. Lee, K. D. Mackenzie, D. Johnson, J. N. Sasserath, S. J. Pearton, F. Ren, Low temperature silicon nitride and silicon dioxide film processing by inductively coupled plasma chemical vapor deposition. *J. Electrochem. Soc.* **147**, 1481 (2000).
38. T. T. Tran, C. Elbadawi, D. Totonjian, C. J. Lobo, G. Grosso, H. Moon, D. R. Englund, M. J. Ford, I. Aharonovich, M. Toth, Robust multicolor single photon emission from point defects in hexagonal boron nitride. *ACS Nano* **10**, 7331–7338 (2016).
39. A. M. Berhane, K.-Y. Y. Jeong, C. Bradac, M. Walsh, D. Englund, M. Toth, I. Aharonovich, Photophysics of GaN single-photon emitters in the visible spectral range. *Phys. Rev. B* **97**, 165202 (2018).
40. L. Jiang, X. Zeng, X. Zhang, The effects of annealing temperature on photoluminescence of silicon nanoparticles embedded in SiNx matrix. *J. Non Cryst. Solids* **357**, 2187–2191 (2011).
41. L. V. Goncharova, P. H. Nguyen, V. L. Karner, R. D'Ortenzio, S. Chaudhary, C. R. Mokry, P. J. Simpson, Si quantum dots in silicon nitride: Quantum confinement and defects. *J. Appl. Phys.* **118**, 224302 (2015).
42. D. Hiller, A. Zelenina, S. Gutsch, S. A. Dyakov, L. López-Conesa, J. López-Vidrier, S. Estradé, F. Peiró, B. Garrido, J. Valenta, M. Kořínek, F. Trojánek, P. Malý, M. Schnabel, C. Weiss, S. Janz, M. Zacharias, Absence of quantum confinement effects in the photoluminescence of Si 3N4-embedded Si nanocrystals. *J. Appl. Phys.* **115**, 204301 (2014).
43. B. Sain, D. Das, Tunable photoluminescence from nc-Si/a-SiNx:H quantum dot thin films prepared by ICP-CVD. *Phys. Chem. Chem. Phys.* **15**, 3881–3888 (2013).
44. J. Martin, F. Cichos, F. Huisken, C. Von Borczyskowski, Electron-phonon coupling and localization of excitons in single silicon nanocrystals. *Nano Lett.* **8**, 656–660 (2008).
45. T. Schmidt, A. M. A. I. Chizhik, A. M. A. I. Chizhik, K. Potrick, A. J. Meixner, F. Huisken, Radiative exciton recombination and defect luminescence observed in single silicon nanocrystals. *Phys. Rev. B* **86**, 125302 (2012).
46. A. M. Chizhik, A. I. Chizhik, R. Gutbrod, A. J. Meixner, T. Schmidt, J. Sommerfeld, F. Huisken, Imaging and spectroscopy of defect luminescence and electron-phonon coupling in single SiO2 nanoparticles. *Nano Lett.* **9**, 3239–3244 (2009).
47. F. T. Rabouw, N. M. B. Cogan, A. C. Berends, W. van der Stam, D. Vanmaekelbergh, A. F. Koenderink, T. D. Krauss, C. de Mello Donega, Non-blinking single-photon emitters in silica. *Sci. Rep.* **6**, 21187 (2016).
48. A. Neumann, J. Lindlau, S. Thoms, T. Basché, A. Högele, Accidental contamination of substrates and polymer films by organic quantum emitters. *Nano Lett.* **19**, 3207–3213 (2019).
49. H. K. Lo, M. Curty, K. Tamaki, Secure quantum key distribution. *Nat. Photonics* **8**, 595–604 (2014).
50. X. L. Chu, S. Götzinger, V. Sandoghdar, A single molecule as a high-fidelity photon gun for producing intensity-squeezed light. *Nat. Photonics* **11**, 58–62 (2017).
51. H. Siampour, S. Kumar, V. A. Davydov, L. F. Kulikova, V. N. Agafonov, S. I. Bozhevolnyi, On-chip excitation of single germanium vacancies in nanodiamonds embedded in plasmonic waveguides. *Light Sci. Appl.* **7**, 61 (2018).
52. D. D. Awschalom, R. Hanson, J. Wrachtrup, B. B. Zhou, Quantum technologies with optically interfaced solid-state spins. *Nat. Photonics* **12**, 516–527 (2018).
53. S. I. Bogdanov, M. Y. Shalaginov, A. S. Lagutchev, C.-C. Chiang, D. Shah, A. S. Baburin, I. A. Ryzhikov, I. A. Rodionov, A. V. Kildishev, A. Boltasseva, V. M. Shalaev, Ultrabright room-temperature sub-nanosecond emission from single nitrogen-vacancy centers coupled to nanopatch antennas. *Nano Lett.* **18**, 4837–4844 (2018).
54. C. C. Chiang, S. I. Bogdanov, O. A. Makarova, X. Xu, S. Saha, D. Shah, Z. O. Martin, D. Wang, A. S. Lagutchev, A. V. Kildishev, A. Boltasseva, V. M. Shalaev, Chip-compatible quantum plasmonic launcher. *Adv. Opt. Mater.* **8**, 2000889 (2020).

Acknowledgments

Funding: This work is supported by the U.S. Department of Energy (DOE), Office of Science through the Quantum Science Center (QSC), a National Quantum Information Science Research Center, and NSF ECCS grant 2015025-ECCS. **Author contributions:** A.S. conceived and planned the experiments. S.P., Z.O.M., and A.S. performed SiN film depositions. S.P. conducted ellipsometry measurements and ellipsometry data analysis. S.P. and Z.O.M. performed thermal annealing of the samples. A.S.L. and D.S. built the optical setup. A.S., Z.O.M., and D.S. performed the optical measurements. A.S. processed the experimental data and performed the analysis. X.X. performed the AFM measurements and fabricated markers by FIB. A.S. wrote the manuscript with support from A.S.L., A.B., and V.M.S. and contributions from all coauthors. A.B. and V.M.S. were in charge of overall direction and planning. All authors discussed the results and commented on the manuscript. **Competing interests:** The authors are inventors on a provisional patent application related to this work filed by the Purdue Research Foundation (no. 63/170,569, filed 5 April 2021). The authors declare that they have no other competing interests. **Data and materials availability:** All data needed to evaluate the conclusions in the paper are present in the paper and/or the Supplementary Materials.

Submitted 21 April 2021
Accepted 25 October 2021
Published 10 December 2021
10.1126/sciadv.abj0627

Room-temperature single-photon emitters in silicon nitride

Alexander SenichevZachariah O. MartinSamuel PeanaDemid SychevXiaohui XuAlexei S. LagutchevAlexandra BoltassevaVladimir M. Shalaev

Sci. Adv., 7 (50), eabj0627. • DOI: 10.1126/sciadv.abj0627